DYNAMICAL SUBSTITUTES OF EQUILIBRIUM POINTS OF ASTEROIDS UNDER SOLAR RADIATION PRESSURE

Xiaosheng Xin[(1)], Daniel J. Scheeres[(2)], Xiyun Hou[(3)], and Lin Liu[(4)]

[(1)(3)(4)]*School of Astronomy and Space Science, Nanjing University, Nanjing, Jiangsu 210023, China, xiaoshengxin@outlook.com*

[(2)]*Department of Aerospace Engineering Sciences, University of Colorado at Boulder, Boulder, CO 80309, USA, scheeres@colorado.edu*

Abstract: *Previous works have focused on the hovering points [1] or periodic motion [2] for an imperfect solar sail near an asteroid with the Hill approximation. Equilibrium points and the associated invariant manifolds of a rotating nonspherical asteroid has also been investigated and the landing trajectories and maneuver strategies have been designed for specific asteroid [3]. In the current study, we analyse the equivalent equilibrium points, i.e., dynamical substitutes of an asteroid under solar radiation pressure (SRP) in the asteroid rotating frame. The uniformly rotating triaxial ellipsoid is adopted to model the gravitation of the asteroid. First, the equations of motion with SRP included are constructed in the rotating frame and are then expanded with respect to the original equilibrium points without considering SRP to obtain the linearised equation for the dynamical substitutes. The linearised solutions are numerically corrected to compute the dynamical substitute orbits. Second, the stability properties of the dynamical substitutes are inspected by calculating the corresponding eigenvalues of the Monodromy matrix. Throughout our analyses, the parameters of the triaxial ellipsoid model of the asteroid, such as the mass, size and period, and those corresponding to the SRP, such as the size of the solar panel, are all taken into account and varied in order to fully evaluate the possible results.*

Keywords: *Asteroid, Dynamical Substitute, Equilibrium Points, Solar Radiation Pressure.*

1. Introduction

Over the last two decades, there have been enduring and increasing interests in asteroid exploration among different countries and space agencies. The Near Earth Asteroid Rendezvous (NEAR) Shoemaker spacecraft rendezvoused with 433 Eros in 2001 [4]; the Chang'e-2 spacecraft made a close flyby of 4179 Toutatis and conducted the first space-borne observation of the asteroid [5]; the OSIRIS-REx mission due to launch in 2016 will visit the carbonaceous, near-Earth asteroid 101955 Bennu in 2018 [6] and so on. For maximum science return of these missions, close orbits around the asteroids need to be adopted by the spacecraft. Apart from the gravitational force of the asteroid, the solar radiation pressure (SRP) and gravitational perturbation of the sun are major factors influencing the dynamics of the spacecraft and these perturbation forces, in particular, the SRP, can be leveraged to design exploration orbits around the asteroid. Hovering points [1] and periodic orbits [2] for solar sail have been devised in the Hill approximation model. Heliotropic orbits with SRP balanced with J2 term of the asteroid gravity field is also constructed [7]. In this paper, we focus on the equilibrium points of asteroids and their corresponding dynamics under SRP.

Nominally, equilibrium points exist in the gravitational potential field of the asteroid. For the triaxial ellipsoid model for the asteroid, there are two types of equilibrium points [8]. Ideally, spacecraft

placed at these equilibrium points will naturally remain there forever. However, with SRP taken into consideration, the equilibrium points will no longer exist. We construct the periodic orbits termed as "dynamical substitutes" under the effect of SRP, which are equivalent to equilibrium points considering only gravity of the asteroid. In Section 2, we present the dynamical model. In Section 3 we illustrate the computation method and obtain families of dynamical substitutes for different combination of parameters. Then the corresponding stability of the dynamical substitutes are analysed and discussions are put forward. We conclude in Section 4.

2. Dynamical Model

For preliminary study, we have made several assumptions to simplify our model. The asteroid is assumed to be a triaxial ellipsoid uniformly rotating about its maximum moment of inertia. The asteroid also revolves around the Sun in a circular orbit with orbital radius r_s equal to 1 AU and the orbital plane coincides with that of the asteroid rotation. The solar array of the spacecraft is considered to be oriented perpendicular to the direction of the Sun and is in perfect absorption.

The problem is constructed in the asteroid-centered rotating coordinate frame. The x axis points along the asteroid longest axis, the z axis along the rotational axis and the y axis completes the right-handed system. The three semi-axes are a, b and c, respectively, and $a \geq b \geq c$. With a taken as the length unit, the three normalized semi-axes of the ellipsoid are denoted as α, which is always equal to unity, β and γ. The time unit is taken as $T/2\pi$ where T is the asteroid rotation period so the nondimensional time is $\tau = (2\pi/T)t$. We also fix the fix the asteroid semi-major axis $a = 1$ km and density $\rho = 2.5$ g cm^{-3}.

The nondimentional equation of motions (EOMs) involving only the gravitation of the asteroid are

$$\begin{cases} \ddot{x} - 2\dot{y} = \dfrac{\partial U}{\partial x} \\ \ddot{y} + 2\dot{x} = \dfrac{\partial U}{\partial y} \\ \ddot{z} = \dfrac{\partial U}{\partial z}, \end{cases} \tag{1}$$

where the effective potential U is defined as

$$U = \frac{1}{2}(x^2 + y^2) - \delta V, \tag{2}$$

$$V = \frac{3}{4}\int_{\lambda}^{\infty} \phi(x,y,z;\nu)\frac{\mathrm{d}\nu}{\Delta(\nu)}, \tag{3}$$

$$\Delta(\nu) = \sqrt{(1+\nu)(\beta^2+\nu)(\gamma^2+\nu)}, \tag{4}$$

$$\phi(x,y,z;\nu) = \frac{x^2}{1+\nu} + \frac{y^2}{\beta^2+\nu} + \frac{z^2}{\gamma^2+\nu} - 1, \tag{5}$$

$$\phi(x,y,z;\lambda)=0, \tag{6}$$

and

$$\delta=\frac{\mu}{\omega^2 a^3}. \tag{7}$$

The gravitational parameter of the asteroid $\mu = GM$ where G is the gravitational constant and M is the mass of of the ellipsoid. δV is the normalized potential of the ellipsoid.

There are usually two types of equilibrium points in this model: the saddle points and the center points which both appear in pairs in the $x-y$ plane. The saddle equilibrium points lie along the semi-major axis and are unstable, whereas the centre points lie on the semi-minor axis and the stability of which is used to categorize the asteroid into 'Type I' (stable center points) or 'Type II' (unstable center points) [8].

The linear stability of the equilibrium points can be determined from the solutions to the variational equations expanded about these points [8, 9]. The planar variational equations are

$$\begin{cases} \ddot{\xi}-2\dot{\eta}=l\xi \\ \ddot{\eta}+2\dot{\xi}=m\eta \\ \ddot{\zeta}=n\zeta \end{cases} \tag{8}$$

in which

$$l=\left.\frac{\partial^2 U}{\partial x^2}\right|_E \quad m=\left.\frac{\partial^2 U}{\partial y^2}\right|_E \quad \text{and} \quad n=\left.\frac{\partial^2 U}{\partial z^2}\right|_E \tag{9}$$

both evaluated at the equilibrium points.Note that $n<0$ is always valid and therefore the motion in the vertical direction is always stable. We only need to investigate the equation set composed of the first two equations. The corresponding characteristic equation is

$$\lambda^4+(4-l-m)\lambda^2+lm=0. \tag{10}$$

The solution is $\Lambda=\lambda^2$

$$\Lambda_{1,2}=\frac{-(4-l-m)\pm\sqrt{(4-l-m)^2-4lm}}{2} \tag{11}$$

For the stable center points, $\Lambda<0$ and

$$\lambda_{1,2}=\pm i(\sqrt{-\Lambda_1})=\pm i\omega_{\text{short}}, \quad \lambda_{3,4}=\pm i(\sqrt{-\Lambda_2})=\pm i\omega_{\text{long}}, \tag{12}$$

in which ω_{long} and ω_{short} are the two intrinsic frequency of the system and $\omega_{\text{short}}<\omega_{\text{long}}$. In Fig. 1, we show the stability of the center points with different rotation periods and geometries of the asteroid. The curves correspond to the 'critical rotation periods' for certain choices of asteroid geometries, some of the values being listed in Tab. 1. The regions above and below each curve correspond to the parameter space where the center points are stable and unstable, respectively. As the rotation period decreases, the center points generally become unstable.

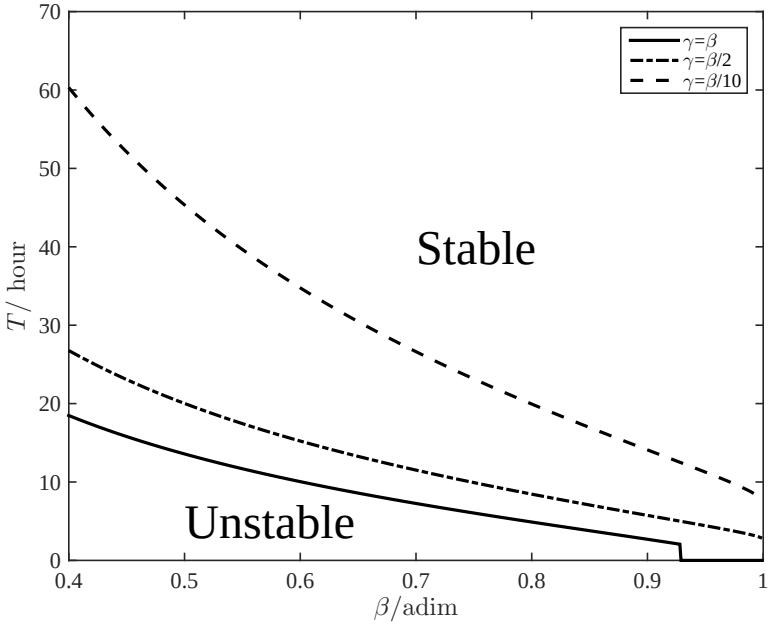

Figure 1. Stability of the center points

Table 1. Rotation periods for different shapes of ellipsoid

Ellipsoid shape ($\beta:\gamma$)	Critical rotation period (h)	Resonant rotation period (h)
0.9:0.6	4.56	5.05
0.8:0.6	6.39	7.65
0.7:0.6	8.18	10.18
0.6:0.6	10.05	12.77

For SRP, its potential form is taken as

$$R_s = -\frac{\kappa}{|\boldsymbol{\delta}|} \tag{13}$$

where $\boldsymbol{\delta} = \boldsymbol{r} - \boldsymbol{r}_s$ and $\boldsymbol{r}$ and $\boldsymbol{r}_s$ are the position vectors of the spacecraft and the sun with respect to the asteroid center. The SRP parameter is

$$\kappa = \nu P_s r_s^2 \sigma \tag{14}$$

in which $P_s = 4.56\ \mu\text{N m}^{-2}$ is the solar pressure exerted on a perfectly absorbing solar array at 1 AU [10], σ is the area-to-mass ratio of the spacecraft and ν is the eclipse factor. Since $|\boldsymbol{r}| \ll r_s$, the potential can be approximated to second-order as

$$R_s = -\frac{\kappa}{r_s^3}\boldsymbol{r}\cdot\boldsymbol{r}_s + \frac{\kappa}{2r_s^3}\left[\boldsymbol{r}\cdot\boldsymbol{r} - 3(\boldsymbol{r}\cdot\hat{\boldsymbol{r}}_s)^2\right] \tag{15}$$

in which $\hat{\boldsymbol{r}}_s = \boldsymbol{r}_s/r_s$. In comparison, under the same approximation condition, the gravitational perturbation of the sun is

$$R_{sun} = -\frac{\mu_s}{2r_s^3}\left[\boldsymbol{r}\cdot\boldsymbol{r} - 3(\boldsymbol{r}\cdot\hat{\boldsymbol{r}}_s)^2\right]. \tag{16}$$

The solar gravitational parameter $\mu_s = 1.3272 \times 10^{11}$ km^3 s^{-2} and $\kappa = 1.026 \times 10^7$ km^3 s^{-2}. Therefore, for a spacecraft with $\sigma = 0.1$ m^2 kg^{-1}, the gravitational perturbation of the sun is approximately three orders of magnitude smaller than the first term of the SRP but much larger than the second term. For our dynamical model, we can only keep the first term of the SRP and neglect the effect of the gravitational perturbation of the sun. The planar EOM considering the SRP are

$$\begin{cases} \ddot{x} - 2\dot{y} = \dfrac{\partial U}{\partial x} + \dfrac{\rho_s}{r_s^2}\cos(\phi + \pi) \\ \ddot{y} + 2\dot{x} = \dfrac{\partial U}{\partial y} + \dfrac{\rho_s}{r_s^2}\sin(\phi + \pi) \end{cases} \tag{17}$$

where $\rho_s = \kappa/(\omega^2 a^3)$ is the normalized SRP parameter and $\phi = -\omega_s \tau + \phi_0$ is the phase angle of the sun with ϕ_0 being the initial value. $\omega_s = 1 - n_s/\omega$ is the nondimensional angular rotation rate of the sun in the asteroid-centered rotation frame and $n_s = 1.16 \times 10^{-5}$ rad s^{-1}.

3. Dynamical substitute and its stability

With the SRP taken into account, Eq. 17 becomes time-dependent and equilibrium points for Eq. 1 no longer exist. These equilibrium points turn into dynamical substitutes, which are periodic orbits around them. Obviously, the period of the dynamical substitute T_d should be equal to that of the additional term arising from the SRP, i.e., $2\pi/\omega_s$. We mainly focus on the dynamical substitutes for the center points in our following study.

3.1. Dynamical substitute

When the SRP is small, the dynamical substitute orbits close enough to the equilibrium point and we can solve for the approximate solution of the dynamical substitute from the variational equations

$$\begin{cases} \ddot{\xi} - 2\dot{\eta} = p\xi - \varepsilon\cos\phi \\ \ddot{\eta} + 2\dot{\xi} = q\eta - \varepsilon\sin\phi \end{cases} \tag{18}$$

in which $\varepsilon = \rho_s/r_s^2$. The solution is

$$\begin{cases} \xi = A_1\cos\phi + B_1\sin\phi \\ \eta = A_2\cos\phi + B_2\sin\phi. \end{cases} \tag{19}$$

with the coefficients

$$\begin{cases} A_1 = \dfrac{m-1}{lm+l+m-3}\varepsilon \\ B_2 = \dfrac{l-1}{lm+l+m-3}\varepsilon \\ A_2 = B_1 = 0 \end{cases} \tag{20}$$

when the condition $lm+l+m-3\neq 0$ is statisfied. The constraint functions for the dynamical substitute are generally

$$\begin{cases} x(T_d+t_0)=x(t_0) \\ y(T_d+t_0)=y(t_0) \\ \dot{x}(T_d+t_0)=\dot{x}(t_0) \\ \dot{y}(T_d+t_0)=\dot{y}(t_0). \end{cases} \tag{21}$$

For the solar eclipse model, we assume that the incoming solar rays are parallel and neglect the penumbra effect. At any given time, the dynamical substitute is at point $P:(x_d,y_d)$ and the phase angle of the sun is ϕ. The boundary of the eclipse is the line l_1, l_2 and l_3. l_1 and l_2 represent the solar rays tangential to the ellipsoid and l_3 connects the two tangential points as shown in Fig. 2. Their functions are

$$\begin{aligned} l_1: &\quad f_1(x,y)=y-k\left(x+\frac{k}{\sqrt{k^2+\beta^2}}\right)-\frac{\beta^2}{\sqrt{k^2+\beta^2}}=0 \\ l_2: &\quad f_2(x,y)=y-k\left(x-\frac{k}{\sqrt{k^2+\beta^2}}\right)+\frac{\beta^2}{\sqrt{k^2+\beta^2}}=0 \\ l_3: &\quad f_3(x,y)=y+\frac{\beta^2}{k}x=0 \end{aligned} \tag{22}$$

where $k=\tan\phi$. The mathematical condition for the eclipse is

$$\nu=\begin{cases} 0 & f_1(x_d,y_d)\cdot f_2(x_d,y_d)\leq 0 \quad \text{and} \quad \sin\phi\cdot f_3(x_d,y_d)\leq 0 \\ 1 & f_1(x_d,y_d)\cdot f_2(x_d,y_d)>0 \quad \text{or} \quad \sin\phi\cdot f_3(x_d,y_d)>0. \end{cases} \tag{23}$$

We adopt differential correction method to numerically solve the constraint functions Eq. 21 for the initial state of the dynamical substitute with

$$\begin{cases} x(t_0)=x_E+\xi(t_0) \\ y(t_0)=y_E+\eta(t_0) \\ \dot{x}(t_0)=\dot{\xi}(t_0) \\ \dot{y}(t_0)=\dot{\eta}(t_0) \end{cases} \tag{24}$$

serving as the initial guess. We generally require the discontinuity between the final and the initial states does not exceed 10^{-11} in nondimensional unit. The initial guess is only valid for small SRP perturbation. For the larger SRP, we obtain the dynamical substitutes through continuation method. Figure 3 shows a family of dynamical substitutes under the effect of increasing SRP. The red ellipse in the figure represents the $x-y$ projection of the ellipsoid.

3.2. Stability of dynamical substitutes

We analyse the stability of the dynamical substitutes by evaluating the eigenvalues of the associated monodromy matrix. For the periodic dynamical substitute, the monodromy matrix is defined as

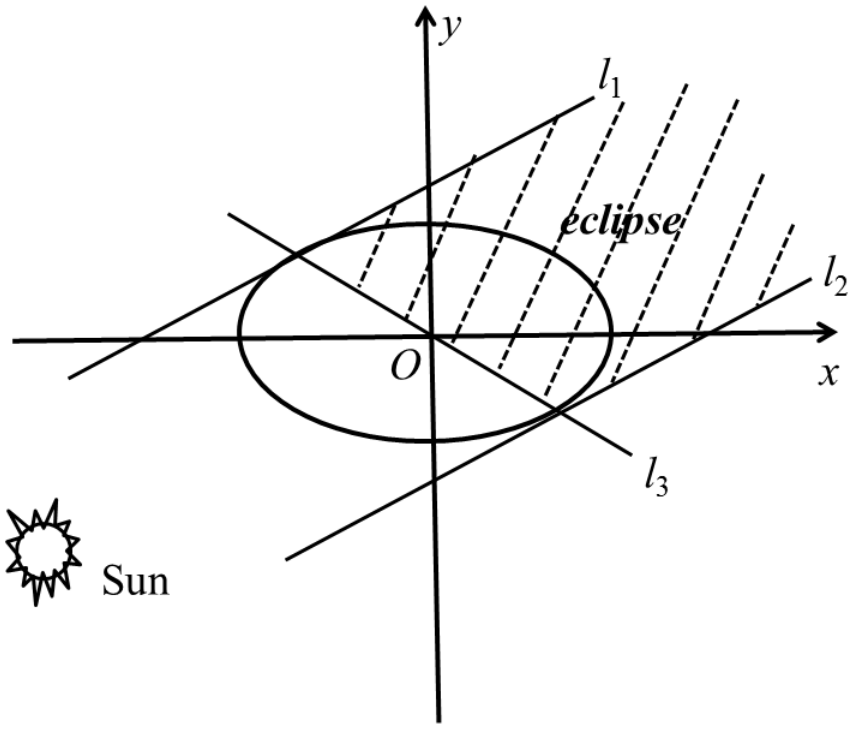

Figure 2. Schematic diagram of eclipse geometry

the state transition matrix (STM) over one period. Generally, for certain cases, the eigenvalues of the monodromy matrix come in pairs which are conjugate as well as reciprocal like

$$\lambda, \frac{1}{\lambda}, \overline{\lambda}, \frac{1}{\overline{\lambda}} \tag{25}$$

in which λ is complex and the module $|\lambda| \geq 1$. For some other cases, the eigenvalues have the form

$$\lambda, \frac{1}{\lambda}, e^{\pm \mathrm{i}u} \tag{26}$$

in which λ and u is real and $|\lambda| > 1$. For stable dynamical substitute, all the modules of the eigenvalues are equal to one, i.e., $|\lambda| = 1$. For the unstable dynamical substitute, the module of the eigenvalues $|\lambda|$ will be larger than one.

For our dynamical model (Eq. 17), there are four free parameters, i.e., β, γ, σ, T. With each pair of (β, γ), the selection of a pair of (σ, T) will yield one dynamical substitute. We search the parameter space of (σ, T) to obtain the stability map of the dynamical substitutes for certain ellipsoid shape (β, γ), which we select four pairs, i.e., $(0.9, 0.6)$, $(0.8, 0.6)$, $(0.7, 0.6)$ and $(0.6, 0.6)$. Fig. 4 shows the four stability maps. The blue and red regions corresponds to the parameter space where the dynamical substitute is stable and unstable, respectively. The white space left is the parameter space where either the dynamical substitute intersects with the ellipsoid or the corresponding

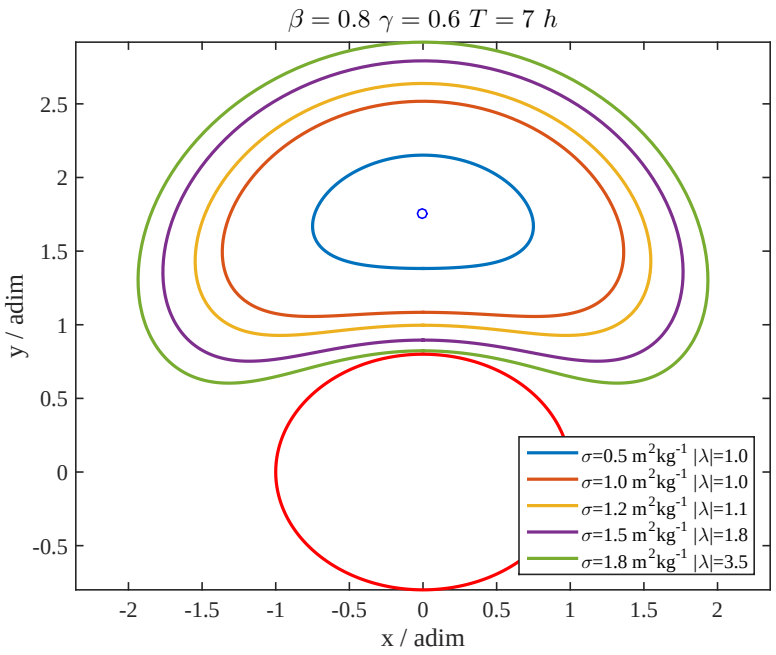

Figure 3. A family of dynamical substitutes

center point lies inside the ellipsoid, the case when we assume the dynamical substitute no longer exists. The different forms of the eigenvalue for the unstable dynamical substitutes corresponding to different types of center points are listed in Tab. 2.

Table 2. Eigenvalue forms for unstable dynamical substitutes

Stability type of center point	Eigenvalue form for unstable dynamical sustitute
stable	$(\lambda, 1/\lambda, e^{\pm i\mu})$, λ is real and $\|\lambda\| > 1$
unstable	$(\lambda, 1/\lambda, \overline{\lambda}, 1/\overline{\lambda})$, λ is complex and $\|\lambda\| > 1$

One unique feature in all four stability maps is the red gap in the stable blue regions. We specially designate the rotation period where the base of the gap lies at the 'resonant rotation period' for which the values are listed in Tab. 1. At this rotation period, the smallest magnitude of the SRP is needed to achieve the transition for the dynamical substitutes from stable state to unstable state. This is due to the effect of the 2:1 resonance between the frequency of the external SRP ω_s and the frequency of the center point ω_{long}.

Another feature is that there exist these blue stable regions in figures for the $(0.7, 0.6)$ and $(0.6, 0.6)$ ellipsoids where the rotation periods are smaller than the corresponding 'critical rotation periods'. This indicates that for ellipsoids that are more elongated, we can actually find the stable dynamical substitutes for the corresponding unstable center points.

By expanding the monodromy matrix to 6D, we can further investigate the vertical stability of the planar dynamical substitutes in addition to the planar stability. Fig. 5 shows the stability map. The red and blue regions indicate that dynamical substitutes are both planar and vertically unstable and stable, respectively. The cyan regions represent the dynamical substitutes which are planar unstable

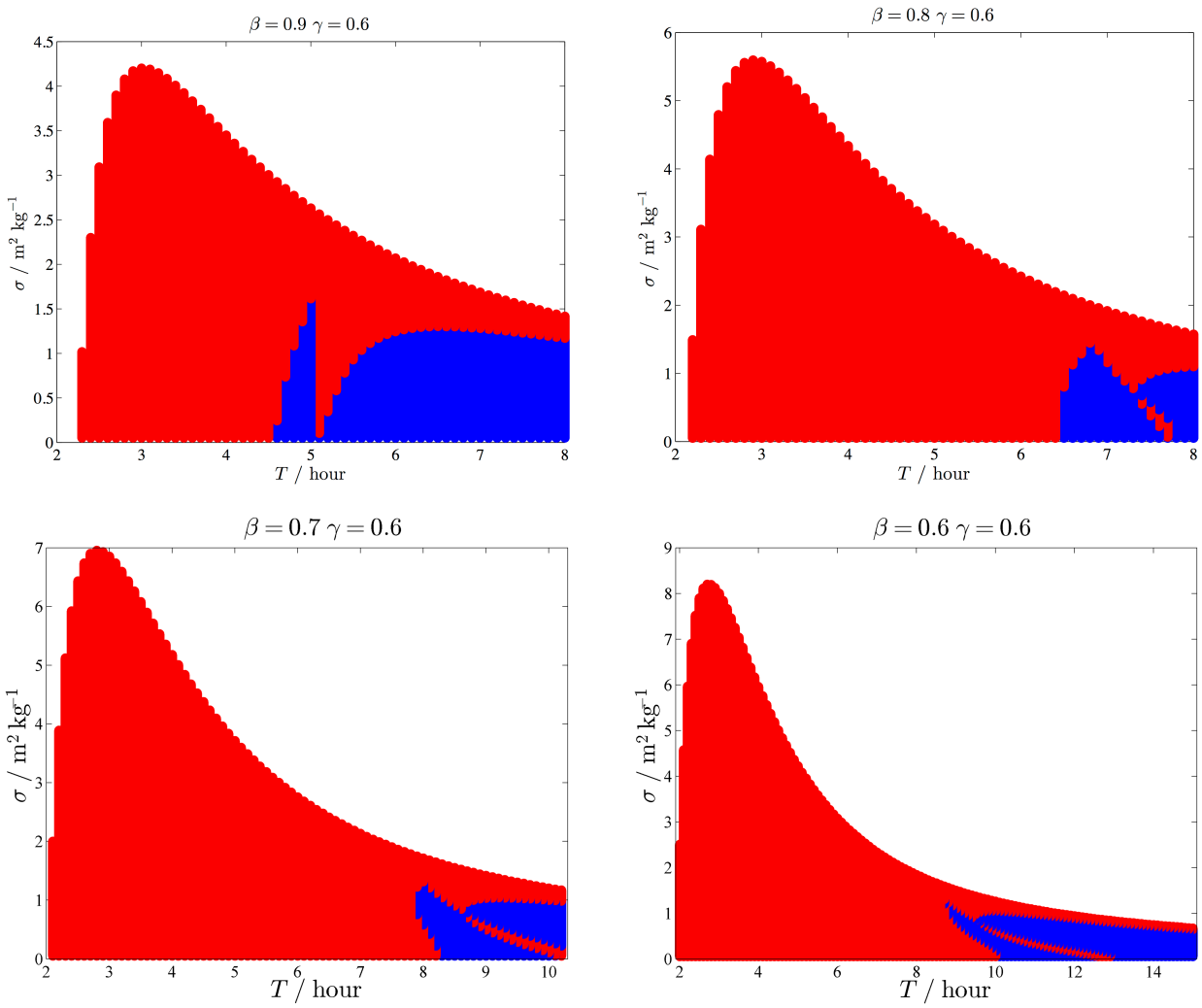

Figure 4. Stability maps of dynamical substitutes of different ellipsoid shapes

but vertically stable, whereas the green regions represent the dynamical substitutes which are planar stable but vertically unstable. For the vertically stable case the third pair of the eigenvalues are $e^{\pm \mathrm{i}\nu}$ and for the vertically unstable case the eigenvalues are $(\lambda, 1/\lambda)$ where λ is real and $|\lambda| > 1$. It is evident from Fig. 5 that for $(0.9, 0.6)$ and $(0.8, 0.6)$ ellipsoids the stable regions are not affected by perturbations in the vertical direction. However, the stable regions further shrinks for $(0.7, 0.6)$ ellipsoid when the vertical stability is taken into account and the stable regions no longer exist for $(0.6, 0.6)$ ellipsoid. Luckily, there are still stable dynamical substitutes of the $(0.7, 0.6)$ ellipsoid corresponding to unstable center points.

4. Conclusion

We model the asteroid as a uniformly rotating triaxial ellipsoid, and considering the effect of SRP perturbation, we compute families of dynamical substitutes, which are equivalent to the equilibrium points in the time-invariant dynamical system.

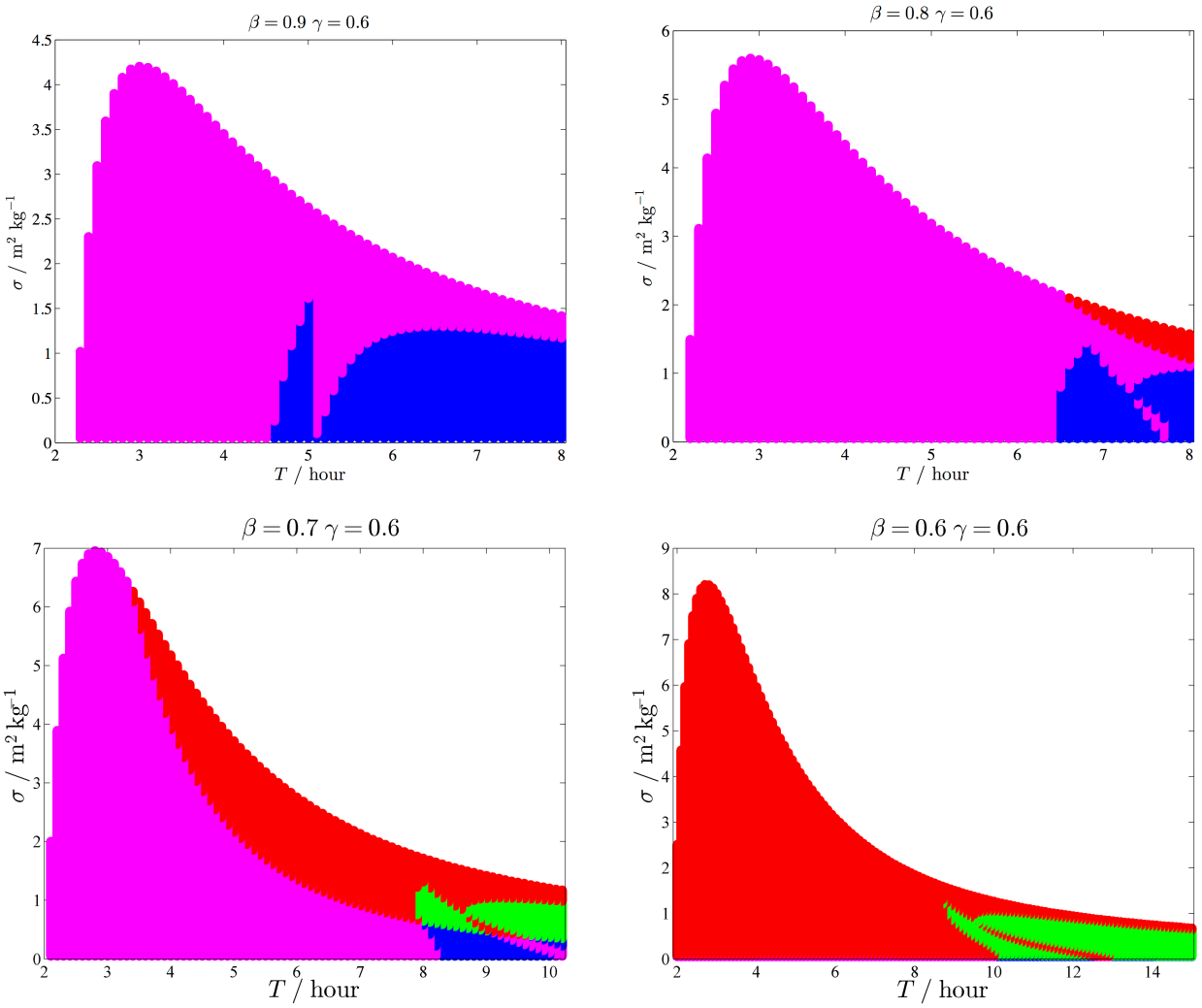

Figure 5. 3D stability maps of planar dynamical substitutes of different ellipsoid shapes

Different geometries and rotation periods of the asteroids as well as the magnitudes of the SRP perturbation are taken into account and how those factors influence the stability of the dynamical substitutes are investigated and shown in the stability maps. Two features clearly stand out: one is the steep drop at the resonant rotation periods when the smallest magnitude of SRP is needed for the stability transition of the dynamical substitutes; another is the existence of stable regions for dynamical substitutes of asteroids with rotation periods below the critical rotation period when the associated center points become unstable. When vertical stability is also considered, stable regions for the dynamical substitutes shrinks as the ellipsoid becomes more elongated.

To better understand the dynamics of equilibrium points and dynamical substitutes of asteroid modelled as ellipsoid, future work should extend the numerical computation to 3D case and the effect of out-of-plane SRP perturbation needs to be accounted for in the dynamical model.

5. References

[1] Morrow, E., Scheeres, D. J., and Lubin, D. "Solar Sail Orbit Operations at Asteroids." Journal of Spacecraft and Rockets, Vol. 38, No. 2, pp. 279–286, 2001.

[2] Macdonald, M., editor. Advances in Solar Sailing. Springer Praxis, Chichester, UK, 2014.

[3] Herrera-Sucarrat, E., Palmer, P. L., and Roberts, R. M. "Asteroid Observation and Landing Trajectories Using Invariant Manifolds." Journal of Guidance, Control, and Dynamics, Vol. 37, No. 3, pp. 907–920, 2014.

[4] Yeomans, D., Antreasian, P., Barriot, J.-P., Chesley, S., Dunham, D., Farquhar, R., Giorgini, J., Helfrich, C., Konopliv, A., McAdams, J., et al. "Radio science results during the NEAR-Shoemaker spacecraft rendezvous with Eros." Science, Vol. 289, No. 5487, pp. 2085–2088, 2000.

[5] Huang, J., Ji, J., Ye, P., Wang, X., Yan, J., Meng, L., Wang, S., Li, C., Li, Y., Qiao, D., et al. "The ginger-shaped asteroid 4179 toutatis: New observations from a successful flyby of Chang'e-2." Scientific Reports, Vol. 3, p. 3411, 2013.

[6] Lauretta, D. S. and OSIRIS-Rex Team. "An overview of the OSIRIS-REx asteroid sample return mission." "Lunar and Planetary Science Conference," Vol. 43, p. 2491. 2012.

[7] Lantukh, D., Russell, R. P., and Broschart, S. "Heliotropic orbits at oblate asteroids: balancing solar radiation pressure and J2 perturbations." Celestial Mechanics and Dynamical Astronomy, Vol. 121, No. 2, pp. 171–190, 2015.

[8] Scheeres, D. J. "Dynamics about uniformly rotating triaxial ellipsoids: applications to asteroids." Icarus, Vol. 110, No. 2, pp. 225–238, 1994.

[9] Brouwer, D. and Clemence, G. M. Methods of Celestial Mechanics. Academic Press, New York, 1961.

[10] McInnes, C. R. Solar sailing: technology, dynamics and mission applications. Springer-Verlag, London, 1999.